RSC Advances

ROYAL SOCIETY OF CHEMISTRY

www.rsc.org/advances

Covalent Modification of Graphene as 2D Nanofiller for Enhanced Mechanical Performance of Poly(glutamate) Hybrid Gels

Hang Li,[a] Ling-Ying Shi,*[a] Wei Cui,[a] Wei-Wei Lei,[a] Yu-Lin Zhang,[a] Yong-Fu Diao,[a] Rong Ran,*[a] and Wei Ni*[b]

[a] *College of Polymer Science and Engineering, State Key Laboratory of Polymer Materials Engineering, Sichuan University, Chengdu 610065, China. E-mail: shilingying@scu.edu.cn; ranrong@scu.edu.cn*

[b] *New Materials R&D Center, Institute of Chemical Materials, Chinese Academy of Engineering Physics, Mianyang 621000, China. Email: niwei@iccas.ac.cn*

Abstract

Graphene-based materials usually require defined functionalization for biological applications in order to control their physical/colloidal properties and to introduce additional capabilities. Here, poly(glutamate), a competitive polypeptide, is covalently grafted onto the graphene oxide two-dimensional (2D) structure through the combination of amidation reaction and ring-opening polymerization as the nanofiller of a hybrid polypeptide-based organogel with enhanced mechanical performance. The morphologies of the hybrid gels reveal that the modified graphene nanostructures may act as nanoscale skeleton, interfacial adhesive in the hybrid gels with nanofibrous 3D network nanostructure.

Introduction

As a novel two-dimensional single-atom-thick carbon material, graphene has received considerable attention due to its interesting thermal, electronic, optical, mechanical and biomedical properties. Graphene-based materials usually require defined functionalization for biological applications in order to control their physical/colloidal properties and to introduce additional capabilities.[1-4] Compared with the graphene, graphene oxide (GO) sheets as a precursor of graphene are heavily oxygenated,[5] bearing hydroxyl and epoxide functional groups on the basal planes and carbonyl and carboxyl groups located at the sheet edges,[6] which make GO susceptible to facile surface modification by non-covalent interaction or covalent bonding with corresponding modifying reagents.[5, 7-10] Significantly, the modified GO sheets with polymer chains can improve the dispersion within the polymer matrix which is crucial for the development of the graphene/polymer nanocomposites.[8, 11-13]

For the covalent modification of GO platelets with polymers,[14-16] two important methodologies including "grafting to"[17, 18] and "grafting from"[19, 20] are commonly used. Compared with "grafting from" method, the "grafting to" method by directly coupling the polymer chains onto the GO platelets provides a good control of the architectures of the polymers, while it demands high active reaction such as "click chemistry", for example, the polymer-grafted GO nanohybrids.[21-23] Another important case of the "grafting to" method is the amidation reaction between the amino group on the polymer chains and the acyl chlorides on GO derivates.[13, 24, 25] Many polypeptides such as poly(γ-benzyl-L-glutamate) (PBLG), poly(L-lysine) (PLL), poly(l-phenylalanine) (PPA) can be synthesized by ring-opening polymerization (ROP) using α-amine as initiator, and the amine groups are still reactive at the ends of the polypeptides,[26-29] which provide the possibility of grafting these kind of

polypeptides onto the GO platelets by amidation reaction. Moreover, the functionalized GO sheets can be used as special 2D nanofillers to control the gelation behaviors as well as the mechanical properties of some polymer gels. Due to the good dispersion ability of the GO platelets in water, many investigations are devoted to the graphene oxide/polymer hybrid hydrogels.[30] For example, hybrid polymeric hydrogels containing GO platelets by noncovalent interaction between the cyclodextrins functionalized GO and PNIPAM block copolymer and the hybrid graphene inclusion complex may show deceased gelation temperature than the pure block copolymer.[31] However, the synthesis of covalently modified GO platelets with biopolymers bearing the capability to form organogels and the performance of the corresponding polymer-functionalized GO/polymer hybrid organogels are still lack of research.[32]

As a typical synthetic polypeptide, poly(γ-benzyl-L-glutamate) (PBLG) has shown many attractive potential applications including a particular interest especially for biomedical and sustainable materials due to its advantages such as biodegradability, biocompatibility and tunable secondary structures.[26,37-39] The PBLG with different molecular weights can form different secondary structures including α-helices and β-sheets.[33, 34] Especially, the PBLG with α-helical conformation presents as a stiff rod-like polymer which leads to unique solution behaviors such as liquid crystalline ordering and thermoreversible gelation.[34-36] It will be of great interest for the fabrication of a series of PBLG based functional materials to extend the potential applications such as biomedical and tissue engineering with enhanced mechanical or thermal performances.

In this work, the polypeptide PBLG is covalently grafted onto the GO platelets through the combination of amidation reaction and ring-opening polymerization. The gelation behaviors of the GO-*g*-PBLG/PBLG hybrid complex in typical organic solvent are explored and the gelation mechanism is speculated based on the interfacial interaction effect of the polymer-grafted-GO platelet hybrid as novel 2D nanofiller. And the moduli and fracture stresses of the hybrid gels with enhanced performances compared with those of PBLG homopolymer gels are investigated by the dynamic rheological measurements.

Results and discussion

As shown in **Scheme 1a**, two PBLG samples with different molecular weights are synthesized through ROP of γ-benzyl-L-glutamate-N-carboxyanhydride (BLG-NCA). First, the monomer, BLG-NCA, was synthesized from the commercially available γ-benzyl-L-glutamate using the method as reported,[40] and the purified BLG-NCA was characterized by ^{1}H NMR as shown in **Fig.S1a** in ESI†. Using the propylamine as initiator and DMF as solvent, two different molecular-weighted PBLG samples were synthesized through ROP by changing the ratio of initiator to monomer under vacuum condition.[28, 41] The synthesized PBLG samples are characterized by GPC (**Fig. 1a** and **Table 1**) and ^{1}H NMR (**Fig. S1b** in ESI† and **Table 1**). From the GPC results, the relative weight-average molecular weights (M_w) of PBLG-1 and PBLG-2 are 13,700 and 6,400 g/mol, respectively, and the polydispersity index (PDI) are 1.58 and 1.53, respectively. From the ^{1}H NMR results using $CDCl_3$/CF_3COOH as solvents,[42, 43] the values of polymerization degrees of PBLG-1 and PBLG-2 are calculated to be 21 and 9, respectively. From the molecular weight of the repeat

unit (277 g/mol) of PBLG and the degrees of polymerization of PBLG, the absolute number-average molecular weights (M_n) of PBLG-1 and PBLG-2 are calculated to be 5,800 and 2,500 g/mol, respectively.

The secondary structures of the synthesized PBLG-1 and PBLG-2 are determined by Fourier transform infrared spectroscopy (FTIR) and one-dimensional wide-angle X-ray diffraction (1D WAXD) experiments. The FTIR spectra of PBLG-1 and PBLG-2 are shown in **Fig. 1b** and **b'**, the latter is the high resolution FTIR spectra with the wavenumber from 1850 to 1550 cm^{-1}. In both FTIR curves of PBLG-1 and PBLG-2, the absorption peaks at 1731 cm^{-1} corresponding to the C=O stretching of the benzyl ester protecting groups of PBLG blocks are observed. For the PBLG-1, the absorption peaks at 1651 cm^{-1} (amide I: 1650–1660 cm^{-1}) and at 1547 cm^{-1} (amide II: 1540–1550 cm^{-1}) are clearly observed characteristic of the α-helix secondary structure. For PBLG-2, the absorption peaks at 1654 cm^{-1} and at 1546 cm^{-1} for α-helix are observed clearly. Thus, from the FTIR results, the secondary structures of both PBLG-1 and PBLG-2 are dominated by α-helix. Furthermore, the small double peaks at 3450-3500 cm^{-1} indicate the existence of the NH_2 groups at the ends of the PBLG chains.

The 1D WAXD profiles of PBLG-1 and PBLG-2 are shown in **Fig. 1c**. In each profile, a set of peaks with a scattering vector ratio of 1:√3:4 and the primary reflection at q^* = 4.47 nm^{-1} with a *d*-spacing of 1.40 nm are observed, indicating that the α-helix secondary structures occur in both PBLG samples, consistent with the FTIR results. However, the primary reflection peak of PBLG-2 is asymmetrical and a small peak at q^* = 3.70 nm^{-1} is observed characteristic of the β-sheet population. Therefore, the 1D WAXD results indicate

the secondary structure of the PBLG-1 is dominated by α-helix, and that of the PBLG-2 is the mixture of higher α-helix content and less β-sheet population. The two PBLG samples with different molecular weights and secondary structures are used to graft onto the GO platelets.

For the synthesis and characterization of GO-*g*-PBLG, graphene oxide is first synthesized by Hummers method from graphite powder, followed by acylation reaction with $SOCl_2$, and the acyl chloride GO derivative (GO-Cl) is obtained. Acyl chlorination of the GO renders a facile amidation reaction with PBLG through the "grafting to" technique.[13] Then the GO-*g*-PBLG is synthesized through amidation reaction between acyl chlorides of GO and amino groups at the end of the PBLG chains illustrated by **Scheme 1b**. As shown in **Fig. 2a**, the PBLG functionalized GO can uniformly disperse in toluene that is a poor solvent for unmodified GO, which preliminarily and directly demonstrates the successful introduction of PBLG onto GO platelets.

Fig. 2b shows the FTIR spectra of GO, GO-*g*-PBLG-1 and GO-*g*-PBLG-2. The FTIR of GO platelets shows typical O–H stretching vibrations (3430 cm^{-1}), C=O stretching vibrations (1721 cm^{-1}), sp^2 C=C bonds (1628 cm^{-1}), and C–O vibrations (1107 cm^{-1}).[10] In the FTIR spectra of GO-*g*-PBLG-1 and GO-*g*-PBLG-2, new peaks including the C–H stretching vibrations (2920 and 2850 cm^{-1}) and the amide I (1640 cm^{-1}) are observed which indicate the existence of PBLG chains on GO platelets.[10, 44, 45] Moreover, the TGA is performed to assess the grafting densities and the thermal properties of the GO-*g*-PBLG-1 and GO-*g*-PBLG-2. For comparison, the TGA curves of GO-*g*-PBLG-1 and GO-*g*-PBLG-2 together with those of pure GO and PBLG-1 are shown in **Fig. 2c**. The TGA curve of GO presents a 12% weight loss below 100 ^oC attributed to the remove of H_2O molecules in the stacked hydrophilic GO

platelets[10] and a 30 % weight loss between 100 and 260 °C attributed to the pyrolysis of labile oxygen containing groups (hydroxyl, epoxy and carboxylated) on the carbon surface. In the TGA curves of GO-*g*-PBLG-1 and GO-*g*-PBLG-2, a 9% weight loss between 120 and 260 °C is attributed to the pyrolysis of labile oxygen groups on GO platelets. The rapid weight losses between 260 and 420 °C on the TGA curves of GO-*g*-PBLG-1 (22 wt %) and GO-*g*-PBLG-2 (15 wt %) are attributed to the decomposition of the PBLG chains attached to the GO nanosheets, from which the grafting densites (wt_{PBLG}/wt_{GO}) of PBLG on GO platelets of the GO-*g*-PBLG-1 and GO-*g*-PBLG-2 are estimated to be 28 wt % and 18 wt %, respectively. It is needed to point out that calculated grafting densities here might be higher than the exact values, because a few unreacted PBLG chains might still occurred in the grafted products, though we have washed the products several times with abundant DFM. In addition, compared with GO, the relative less weight losses (wt_{loss}/wt_{GO}) of GO-*g*-PBLG-1 (12 wt %) and GO-*g*-PBLG-2 (10 wt %) below 260 °C can be ascribed to the partially reduction of the GO during synthesis process and the increase of the thermal stability because of the PBLG layer inhibiting decomposition of residual groups on GO platelets. In addition, the residual mass of GO-*g*-PBLG-1 (62.1 %) is less than that of GO-*g*-PBLG-2 (68.5 %) which also indicates the overall number of repeat unit of PBLG on GO-*g*-PBLG-1 more than that of GO-*g*-PBLG-2.

X-ray photoelectron spectroscopy (XPS) was employed to investigate the type and nature of elements on the surface of the GO and GO-*g*-PBLG. In the full XPS spectrum of GO-*g*-PBLG-1 and GO-*g*-PBLG-2 as shown in **Fig. 3a**, the N element (400.0 eV) is detected in addition to the C (285.5 eV) and O (532.5 eV) elements, which verifies that PBLG is

successfully grafted on to the GO surfaces. In addition, the C 1s XPS spectra of GO, GO-*g*-PBLG-1 and GO-*g*-PBLG-2 are depicted in **Fig. 3b–d**, respectively, where the C ls peak has been decomposed into different fitting curves. The C 1s peak of GO have four fitting curves with binding energy situated at 284.5, 286.5, 287.5 and 288.5 eV which are assigned to C–C, C–O, C=O and O–C=O, respectively.[12] Compared with the C 1s XPS spectra of GO, the GO-*g*-PBLG-1 and GO-*g*-PBLG-2 have a new peak at 286.3 eV corresponding to C–N binding energy, which once again confirms the successful grafting process. And the relatively intensities of C–O, C=O and O–C=O peaks of GO-*g*-PBLG are much lower than those of the GO which indicate the partial reduction of GO during the reaction process. Moreover, the molar ratios of C:O of GO, GO-*g*-PBLG-1, GO-*g*- PBLG-2 can be calculated to be 2.7, 5.79 and 5.47, respectively, from the elements containing (**Table 2**). The C:O molar ratio of the PBLG is 10:3 obtained from the molecular structure. Thus the C:O molar ratio of the GO-*g*-PBLG is higher than that of both GO and PBLG which also indicates the partial reduction of GO during the reaction process.[16] And the N element content of GO-*g*-PBLG-1 (2.5%) is higher than that of GO-*g*-PBLG-2 (0.8%) also indicating that the grafting density of PBLG on GO-*g*-PBLG-1 is larger than that on GO-*g*-PBLG-2, which is consistent with the TGA results.

Fig. 4 shows the TEM images of GO nanosheets and GO-*g*-PBLG-1. As shown in **Fig. 4a**, the single layered pristine GO sheet with smooth surface is observed, which indicates the successful exfoliation of synthesized GO nanosheets. In the TEM image of GO-*g*-PBLG-1 as shown in **Fig. 4b**, the GO platelets decorated with PBLG aggregates indicated by the dark dots on the GO platelets are observed. It is necessary to point out that the PBLG chains used

should not have so large sized to be observed, thus the dots observed should be the aggregates of PBLG α-helixes. From above, the GO-*g*-PBLG was successfully synthesized and fully characterized, and the good dispersion ability of functionalized GO in toluene is important for the preparation of GO-*g*-PBLG/PBLG hybrid gel in toluene.

To investigated the performances of the hybrid GO-g-PBLG/PBLG organogel, which was prepared according the method described in the ESI and the critical sol-gel transition temperatures and concentrations were determined by tube inversion technology.[46] For the PBLG homopolymer gel, the gelation concentrations of PBLG-1 and PBLG-2 are 0.5 and 1.5 wt %, respectively, and the gelation temperatures of PBLG-1 and PBLG-2 are 49.5 and 47.5 ^{o}C, respectively. The gelation ability of the PBLG is determined by the conformation of PBLG and the α-helical conformation of PBLG is crucial for its thermoreversible gelation.[34, 35] As described previously, the 1D WAXD results indicate that the conformation of PBLG-1 is dominated by α-helix and that of the PBLG-2 is the mixture of α-helix and β-sheet population. Therefore, the PBLG-1 has better gelation ability to form organogel in toluene. And the gelation concentration of PBLG-1 is lower than that of PBLG-2 and the gelation temperature of PBLG-1 is higher than that of PBLG-2.

For the GO-*g*-PBLG/PBLG hybrid complex, it was found find that the hybrid complex containing 0.05 wt % of GO-*g*-PBLG-1 with 0.40 wt % PBLG-1 transformed from solution to gel during cooling process (**Fig. S2** in ESI†), and the gelation temperature was measured to be 50.0 ^{o}C. In the hybrid complex, the overall weight fraction of PBLG should be less than 0.50 wt % which was the gelation concentration of pure PBLG-1. For the GO-*g*-PBLG-2/PBLG-2 complex, the complex containing 0.05 wt % of GO-*g*-PBLG-2 and

1.4 wt % of PBLG-2 hybrid in which the overall concentration of PBLG is also slightly less than the gelation concentration of pure PBLG-2, displays gel state after cooling (**Fig. S2** in ESI†), and the gelation temperature is measured to be 48.3 ^{o}C. The small increase of gelation temperature and the slight decrease of the gelation concentration of the GO-*g*-PBLG/PBLG hybrid complexes demonstrate that the GO platelets do not hamper the gelation ability but slightly trigger the gelation of PBLG.

In order to investigate the gelation mechanism of the hybrid complex and the morphology of the hybrid gel, the TEM experiments were further carried out. As shown in **Fig. 5a**, the pure PBLG-1 gel exhibits the morphologies of aligned and nonaligned fibers and the diameters of the fibers are ranging from ten to hundred nanometers which are much larger than the diameter of the PBLG rods. Thus, the fibers are composed by bundles of nematic ordered PBLG rods which is consistent with the gelation mechanism of PBLG reported in literature.[34, 36] The model of PBLG-1 gel and the molecular arrangement in the fiber is illustrated in **Fig. 5b**. For the GO-*g*-PBLG-1/PBLG-1 hybrid gel as shown in **Fig 5c**, the fibrous network with folded GO platelets is observed. The diameters of the fibers of the GO-g-PBLG/PBLG hybrid gel are on the same scale of the fibers of the PBLG homopolymer gel. As marked by the red circles in the TEM image of Fig 5c, some fibers begin from the edge of the GO platelets which indicate the PBLG brushes of the GO-*g*-PBLG are effectively form fibers with the PBLG homopolymers and some the PBLG grafted GO platelets act as the 2D adhesive for the PBLG fibers. The nanostructure and the molecular arrangement of the GO-*g*-PBLG/PBLG hybrid gel are illustrated by the model shown in **Fig. 5d**. From the above investigations on the gelation behaviors and the gel-morphologies of the GO-g-PBLG/PBLG

hybrid complex, it can be concluded that the aggregation of the PBLG helices still play a key role in the gelation ability of the hybrid complex and GO platelets with PBLG brushes act as 2D nanofillers leading to the GO containing 3D network structure of the hybrid gel.

Finally, the influence of the GO platelets on rheological properties of organogels was studied by dynamic oscillatory stress sweep measurements. In order to avoid the influence of the concentration on rheological properties of the gel, the same overall concentrated PBLG gels and GO-g-PBLG/PBLG hybrid gels were prepared and characterized. **Fig. 6a** shows the stress sweeps from 0.1 to 100 Pa at a constant frequency of 1 Hz of the PBLG-1 gel and GO-*g*-PBLG-1/PBLG-1 hybrid gels with the same overall concentration (0.6 wt %). It is obviously observed that the storage (*G*') and loss (*G*") moduli of both GO-*g*-PBLG-1 (0.05 wt %)/PBLG-1 (0.55 wt %) and GO-*g*-PBLG-1 (0.10 wt %)/PBLG-1 (0.50 wt %) hybrid gels are much larger than those of the PBLG-1 (0.60 wt %) gel, respectively. In addition, when the G″ value is large than the G′ value, the gel is destroyed based on which the fracture stress of the gel can be determined. The fracture stress of the GO-*g*-PBLG-1 (0.05 wt %)/PBLG-1 (0.55 wt %) occurs at 45 Pa and that of GO-*g*- PBLG-1 (0.10 wt %)/ PBLG-1 (0.50 wt %) hybrid gel occurs at 50 Pa, both of which are larger than the fracture stress (35 Pa) of PBLG-1 (0.60 wt %) gel. Moreover, the rheological properties of GO-*g*-PBLG-2/PBLG-2 hybrid gel compared with PBLG-2 homopolymer gel are investigated. As shown in **Fig. 6b**, both the moduli (*G*' and *G*") and the fracture stresses of the GO-*g*- PBLG-2/PBLG-2 hybrid gels are also larger than the corresponding values of the PBLG-2 homogel with the same overall concentration. Therefore, the network of GO-*g*-PBLG/PBLG is more perfect than that

of the corresponding PBLG homopolymer gel, which results to the improved mechanical performances.

Conclusions

In summary, the polypeptide PBLG covalently functionalized graphene oxide platelets have been successfully synthesized by combination of the ring-opening polymerization of BLG-NCA monomer and the amidation reaction. The PBLG grafted GO platelets display good dispersion ability in nonpolar organic solvents such as toluene. For the GO-*g*-PBLG/PBLG hybrid complex as organogel, the GO platelets will act as 2D adhesive triggering the gelation of PBLG with a lower gelation concentration. Considerably, the GO-*g*-PBLG/PBLG hybrid gels show increased moduli and fracture stresses than the PBLG homopolymer counterpart. The synthesis method achieved in this work may provide a general reference for the modification of GO platelets with many other polypeptides for the fabrication of reinforced biocompatible, biodegradable and sustainable gels.

Acknowledgements

Financial supports from the National Natural Science Foundation of China (Grant 51403132) and the Support Plan Projects of Technological Office of Sichuan Province (Grant 2014GZX0010-4) are gratefully acknowledged.

Notes and references

1. a) A. K. Geim, *Science* 2009, **324**, 1530; b) K. S. Kim, Y. Zhao, H. Jang, S. Y. Lee, J. M. Kim, K. S. Kim, J.-H. Ahn, P. Kim, J.-Y. Choi and B. H. Hong, *Nature* 2009, **457**, 706.
2. M. J. Allen, V. C. Tung and R. B. Kaner, *Chem. Rev.* 2010, **110**, 132.
3. A. A. Balandin, S. Ghosh, W. Bao, I. Calizo, D. Teweldebrhan, F. Miao and C. N. Lau, *Nano lett.* 2008, **8**, 902.
4. E. Wang, M. S. Desai, K. Heo and S.-W. Lee, *Langmuir*, 2014, **30**, 2223-2229.
5. D. R. Dreyer, S. Park, C. W. Bielawski and R. S. Ruoff, *Chem. Soc. Rev.* 2010, **39**, 228.
6. J. I. Paredes, S. Villar-Rodil, A. Martínez-Alonso and J. M. D. Tascón, *Langmuir* 2008, **24**, 10560.
7. S. Stankovich, D. A. Dikin, G. H. B. Dommett, K. M. Kohlhaas, E. J. Zimney, E. A. Stach, R. D. Piner, S. T. Nguyen and R. S. Ruoff, *Nature* 2006, **442**, 282.
8. T. Kuilla, S. Bhadra, D. Yao, N. H. Kim, S. Bose and J. H. Lee, *Prog. Polym. Sci.* 2010, **35**, 1350.
9. O. C. Compton and S. T. Nguyen, *Small* 2010, **6**, 711. S. Mallakpour, A. Abdolmaleki and S. Borandeh, *Appl. Surf. Sci.* 2014, **307**, 533.
10. a) S. H. Lee, H. W. Kim, J. O. Hwang, W. J. Lee, J. Kwon, C. W. Bielawski, R. S. Ruoff and S. O. Kim, *Angew. Chem. Int. Ed.* 2010, **49**, 10084; b) H. Bao, Y. Pan, Y. Ping, N. G. Sahoo, T. Wu, L. Li, J. Li and L. H. Gan, *Small* 2011, **7**, 1569.
11. J. Kim, L. J. Cote and J. Huang, *Acc. Chem. Res.* 2012, **45**, 1356.
12. K. W. Putz, O. C. Compton, M. J. Palmeri, S. T. Nguyen and L. C. Brinson, *Adv. Funct. Mater.* 2010, **20**, 3322-3329.

13. a) M.-Y. Lim, H. J. Kim, S. J. Baek, K. Y. Kim, S.-S. Lee and J.-C. Lee, *Carbon* 2014, **77**, 366; b) J. Chu, X. Li and P. Xu, *J. Mater. Chem.* 2011, **21**, 11283.

14. M. Fang, K. Wang, H. Lu, Y. Yang and S. Nutt, *J. Mater. Chem.* 2010, **20**, 1982.

15. H. J. Salavagione, G. Martínez and G. Ellis, *Macromol. Rapid Commun.* 2011, **32**, 1771.

16. Z. Liu, Z. Xu, X. Hu and C. Gao, *Macromolecules* 2013, **46**, 6931.

17. H. J. Salavagione, M. A. Gómez and G. Martínez, *Macromolecules* 2009, **42**, 6331.

18. P. Zhang, K. Jiang, C. Ye and Y. Zhao, *Chem. Comm.* 2011, **47**, 9504.

19. Y. Yang, J. Wang, J. Zhang, J. Liu, X. Yang and H. Zhao, *Langmuir* 2009, **25**, 11808.

20. H. Hu, X. Wang, J. Wang, L. Wan, F. Liu, H. Zheng, R. Chen and C. Xu, *Chem. Phys. Lett.* 2010, **484**, 247.

21. Y. Jing, H. Tang, G. Yu and P. Wu, *Poly. Chem.* 2013, **4**, 2598.

22. S. Sun, Y. Cao, J. Feng and P. Wu, *J. Mater. Chem.* 2010, **20**, 5605.

23. Y. Cao, Z. Lai, J. Feng and P. Wu, *J. Mater. Chem.* 2011, **21**, 9271.

24. D. Meng, S. Yang, L. Guo, G. Li, J. Ge, Y. Huang, C. W. Bielawski and J. Geng, *Chem. Comm.* 2014, **50**, 14345.

25. X. Zhuang, Y. Chen, L. Wang, K.-G. Neoh, E.-T. Kang and C. Wang, *Poly. Chem.* 2014, **5**, 2010.

26. H. R. Kricheldorf, *Angew. Chem. Int. Ed.* 2006, **45**, 5752.

27. H. Iatrou, H. Frielinghaus, S. Hanski, N. Ferderigos, J. Ruokolainen, O. Ikkala, D. Richter, J. Mays and N. Hadjichristidis, *Biomacromolecules* 2007, **8**, 2173.

28. J. Sun, X. Chen, C. Deng, H. Yu, Z. Xie and X. Jing, *Langmuir* 2007, **23**, 8308.

29. L. Yu, W. Fu and Z. Li, *Soft Matter* 2015, **11**, 545.

30. a) S. Sun and P. Wu, *J. Mater. Chem.* 2011, **21**, 4095; b) R. Liu, S. Liang, X.-Z. Tang, D. Yan, X. Li and Z.-Z. Yu, *J. Mater. Chem.* 2012, **22**, 14160.

31. J. Liu, G. Chen and M. Jiang, *Macromolecules* 2011, **44**, 7682.

32. a) S. R. Raghavan and J. F. Douglas, *Soft Matter* 2012, **8**, 8539; b) A. R. Hirst, I. A. Coates, T. R. Boucheteau, J. F. Miravet, B. Escuder, V. Castelletto, I. W. Hamley and D. K. Smith, *J. Am. Chem. Soc.* 2008, **130**, 9113; c) S. E. Kudaibergenov, N. Nuraje and V. V. Khutoryanskiy, *Soft Matter* 2012, **8**, 9302; d) E. Caló and V. V. Khutoryanskiy, *Eur. Polym. J.* 2015, **65**, 252.

33. K. T. Kim, C. Park, G. W. Vandermeulen, D. A. Rider, C. Kim, M. A. Winnik and I. Manners, *Angew. Chem. Int. Edit.* 2005, **117**, 8178.

34. R. Tadmor, R. L. Khalfin and Y. Cohen, *Langmuir* 2002, **18**, 7146.

35. P. Papadopoulos, G. Floudas, H. A. Klok, I. Schnell and T. Pakula, *Biomacromolecules* 2003, **5**, 81.

36. K. Tohyama and W. G. Miller, *Nature* 1981, **289**, 813.

37. K. T. Kim, C. Park, G. W. M. Vandermeulen, D. A. Rider, C. Kim, M. A. Winnik and I. Manners, *Angew. Chem. Int. Ed.* 2005, **117**, 8178.

38. V. K. Kotharangannagari, A. Sánchez-Ferrer, J. Ruokolainen and R. Mezzenga, *Macromolecules* 2012, **45**, 1982.

39. C. Chen, D. Wu, W. Fu and Z. Li, *Aust. J. Chem.* 2014, **67**, 59.

40. D. S. Poché, M. J. Moore and J. L. Bowles, *Synth. Commun.* 1999, **29**, 843.

41. F. Zhou, T. Ye, L. Shi, C. Xie, S. Chang, X. Fan and Z. Shen, *Macromolecules* 2013, **46**, 8253.

42. J. A. Ferretti and B. W. Ninham, *Macromolecules* 1970, **3**, 30.

43. F. A. Bovey, J. J. Ryan, G. Spach and F. Heitz, *Macromolecules* 1971, **4**, 433.

44. T. Kavitha, I.-K. Kang and S.-Y. Park, *Langmuir* 2013, **30**, 402.

45. L. Nguyễn, S.-M. Choi, D.-H. Kim, N.-K. Kong, P.-J. Jung and S.-Y. Park, *Macromol. Res.* 2014, **22**, 257.

46. A. R. Hirst, D. K. Smith, M. C. Feiters, H. P. M. Geurts and A. C. Wright, *J. Am. Chem. Soc.* 2003, **125**, 9010.

Figures and captions

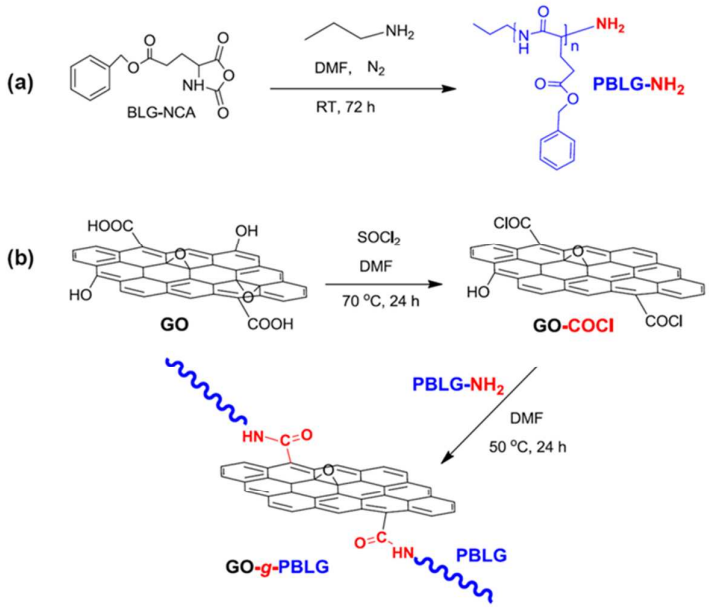

Scheme 1 Schematic illustration of (a) synthesis of functionalized polypeptide PBLG-NH_2 and (b) GO-*g*-PBLG hybrid.

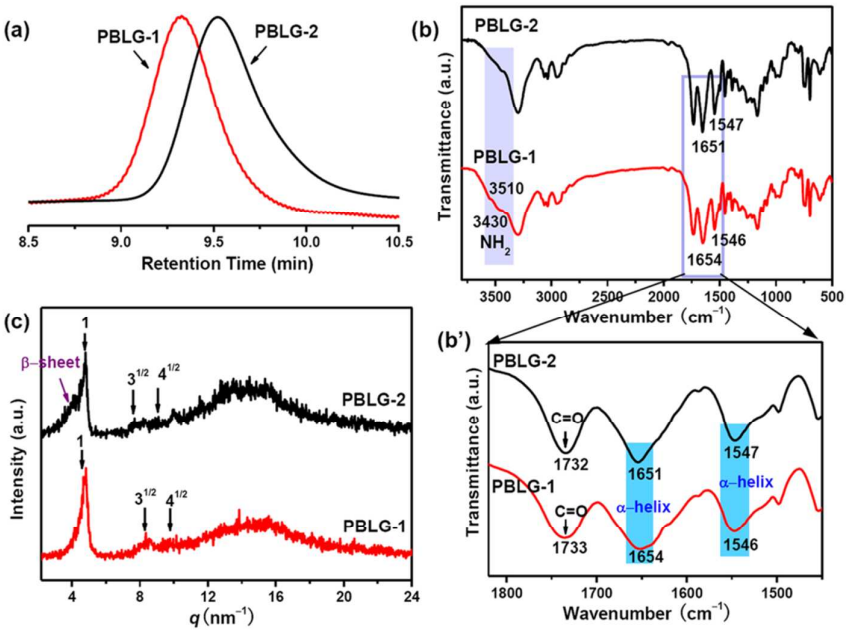

Fig. 1 (a) GPC curves of PBLG-1 and PBLG-2 synthesized, (b and b') FTIR spectra and (c) 1D WAXD profiles of PBLG-1 and PBLG-2 after annealed.

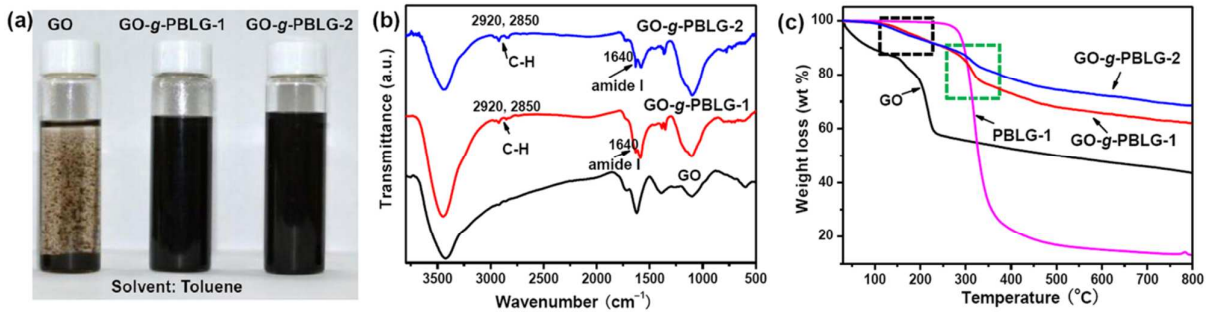

Fig. 2 (a) Digital photographs of GO, GO-*g*-PBLG-1, and GO-*g*-PBLG-2 dispersed in toluene, (b) FTIR spectra and (c) TGA curves of GO, GO-*g*-PBLG-1, and GO-*g*-PBLG-2.

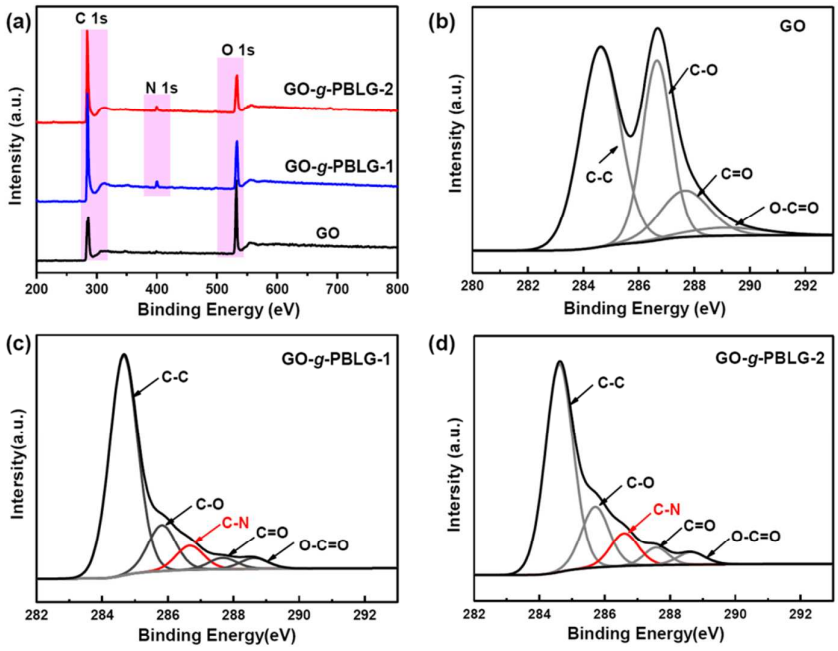

Fig. 3 (a) Wide-scan XPS spectra of GO, GO-*g*-PBLG-1 and GO-*g*-PBLG-2, and (b–d) C 1s core-level spectra of GO, GO-*g*-PBLG-1, and GO-*g*-PBLG-2, respectively.

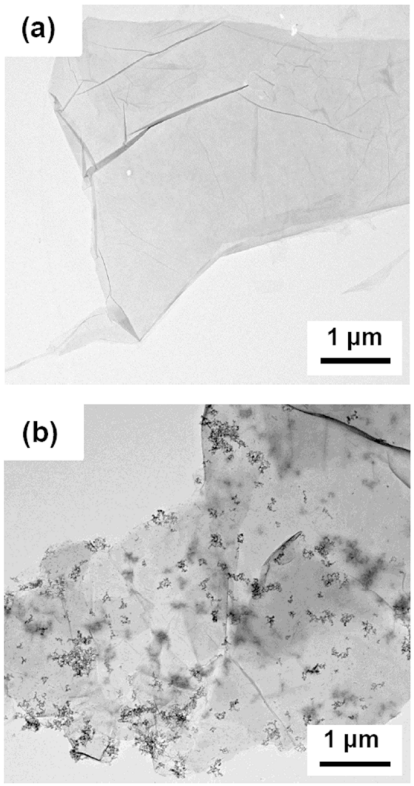

Fig. 4 TEM images of (a) GO and (b) GO-*g*-PBLG-1.

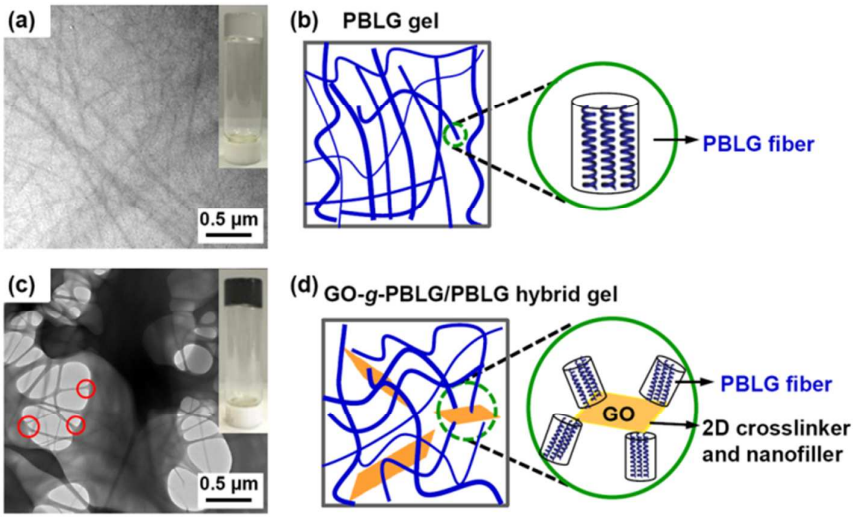

Fig. 5 (a) TEM image of PBLG-1 organogel (0.6 wt % concentration in toluene) with the digital photograph of the gel in the inset, and (b) the model of the fibrous network composed by the bundles of the PBLG helixes. (c) TEM image of GO-*g*-PBLG-1 (0.05 wt %)/PBLG-1 (0.55 wt %) hybrid organogel in toluene with the digital photograph of the hybrid gel in the inset, and (d) the model of the fibrous network composed by the bundles of the PBLG helixes and the 2D nanofiller/adhesive of GO platelets.

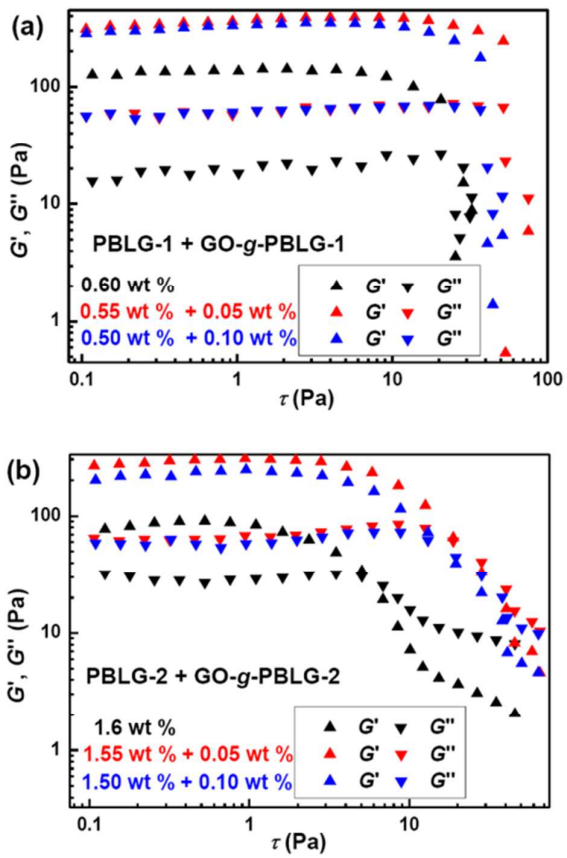

Fig. 6 (a) Storage (G') and loss (G'') moduli of PBLG-1 gel and GO-*g*-PBLG-1/PBLG-1 hybrid gels with indicated compositions at the same overall concentration of 0.60 wt % as a function of stress sweep, and (b) storage (G') and loss (G'') moduli of PBLG-2 gel and GO-*g*- PBLG-2/PBLG-2 hybrid gels with indicated compositions (total concentration of 1.60 wt %) as a function of stress sweep.

Table 1 Molecular Weights, PDIs and Degrees of polymerization of PBLG samples

Samples	M_n [a] (g/mol)	M_w [b] (g/mol)	PDI [b]	Degree of polymerization [a]
PBLG-1	5,800	13.700	1.58	21
PBLG-2	2,500	6.400	1.53	9

[a] Determined from ^{1}H NMR results, and [b]Determined from GPC results.

Table 2 The elements contents and C:O mole ratios of GO, GO-g-PBLG-1 and GO-g- PBLG-2 from XPS results.

Element	C (atom%)	O (atom%)	N (atom%)	C:O
GO	72.99	27.01	0	2.70
GO-*g*-PBLG-1	83.14	14.36	2.50	5.79
GO-*g*- PBLG-2	83.86	15.34	0.80	5.47